International Scientific Conference 20 UNITECH 26

INTERNATIONAL SCIENTIFIC CONFERENCE
19-21 November 2026
GABROVO

# SINGLE-ELECTRON GROUND STATE AND DONOR BINDING IN LATERALLY COUPLED CYLINDRICAL GaAs QUANTUM WELL WIRES UNDER AN ELECTRIC FIELD

**Batu Hunca***

*Department of Physics, Faculty of Science, Trakya University, 22030 Edirne, Türkiye*
**Corresponding author: batuhunca@trakya.edu.tr*

**Abstract**
*In this study, we investigate the electron ground state and the binding energy of a hydrogenic donor in two laterally coupled cylindrical GaAs quantum well wires (QWWs) under an electric field, with the donor position varied along the line joining the wire centres. Calculations are performed using the finite-element method and a variational approach within the effective-mass approximation. The effects of unequal confinement potentials in the two wires on the donor binding energy are examined. The binding energy depends on the confinement profile and the donor position. The ground-state energy reaches its maximum at a different field in each structure, and a donor at the centre of one wire ($x_i = 10.0$ nm) shifts this field by about 7 kV/cm.*

**Keywords: quantum well wire, coupled wires, donor binding energy, electric field, finite element method**

## INTRODUCTION

Tunnel-coupled double quantum dots form an effective two-level system whose energy splitting is set by the device geometry and can be tuned by a gate voltage [1]. Such double dots are the basis of semiconductor spin qubits [2], and coherent control of their charge state has been demonstrated through charge oscillations [3]. Two laterally coupled quantum well wires (QWWs) are the one-dimensional counterpart of this system. Controlling the charge state of a wire pair in the same way requires knowledge of both the value of the control parameter at which the electron transfers between the wires and the sharpness of this transition. Here, the control parameter is the confinement offset or the applied electric field.

Several experimental and theoretical approaches have been used to investigate coupling and interwire transfer. Experimentally, the coupling has been tuned using a barrier gate [4] and extracted from the width of the charge-transfer line [5]. In optical studies, the bonding–antibonding doublet of a coupled-dot pair has been tuned through resonance by an applied field [6]. Lateral-field tuning of coupled dot pairs has also been studied [7,8]. In computational studies, Vinasco *et al.* [9] and Heyn and Duque [10] have used the finite-element method for elliptical GaAs quantum rings and cylindrical GaAs quantum dots, respectively, and laterally coupled circular dots under an applied field have been treated in Ref. [11].

A related body of work concerns donor impurities in QWWs and quantum dots. Donor states in a single cylindrical QWW were computed variationally in Bryant's early work [12]; single and coaxial QWWs were later treated using the same method under laser fields [13,14]. For coupled rectangular QWWs, Tangarife and Duque computed the binding energy under hydrostatic pressure and an applied field [15,16]. Similar calculations have also been performed for laterally coupled dot pairs [17]. Aktaş and co-workers calculated the


*This is an open access article licensed under Creative Commons Attribution 4.0 International*
*Print ISSN: 1313-230X, Online ISSN: 3033-1404*

binding energy of a hydrogenic impurity in a coaxial GaAs QWW under an electric field [18] and under combined electric and magnetic fields [19]. The present work extends these studies to a pair of laterally coupled cylindrical wires.

In this work, we study an electron in two laterally coupled cylindrical GaAs QWWs under an electric field, with and without a hydrogenic donor. The subband states are calculated with the finite-element method, and the donor state is obtained variationally. We consider an equal pair and two pairs in which the potential floor of the left wire is raised. We determine the field at which the electron transfers from one wire to the other, the donor binding energy as a function of donor position, and the shift of the transfer field caused by the donor.

## THEORY

The two wires are parallel to the $z$ axis. Their cross sections lie in the $x$–$y$ plane and are circles of radius $R$ centred at $(\pm d_0, 0)$ on the $x$ axis; the wires are GaAs and the surrounding barrier is $Al_{0.3}Ga_{0.7}As$. An electric field $\mathbf{F} = F\hat{\mathbf{x}}$ is applied perpendicular to the wire axes, along the line joining the wire centres. Within the framework of the effective-mass approximation, the Hamiltonian of an electron bound to a hydrogenic donor in the coupled QWWs is given by

$$H = -\frac{\hbar^2}{2m^*}\nabla^2 + V(x,y) + eFx - \frac{e^2}{4\pi\varepsilon_0\varepsilon_r|\mathbf{r}-\mathbf{r}_i|}, \quad (1)$$

where $m^*$ is the electron effective mass, $e$ is the elementary charge, $\varepsilon_r$ is the static dielectric constant, $V$ is the confinement potential, and $\mathbf{r} = (x, y, z)$ and $\mathbf{r}_i = (x_i, 0, 0)$ are the electron and donor positions. The same $m^*$ and $\varepsilon_r$ are used in the wires and in the barrier.

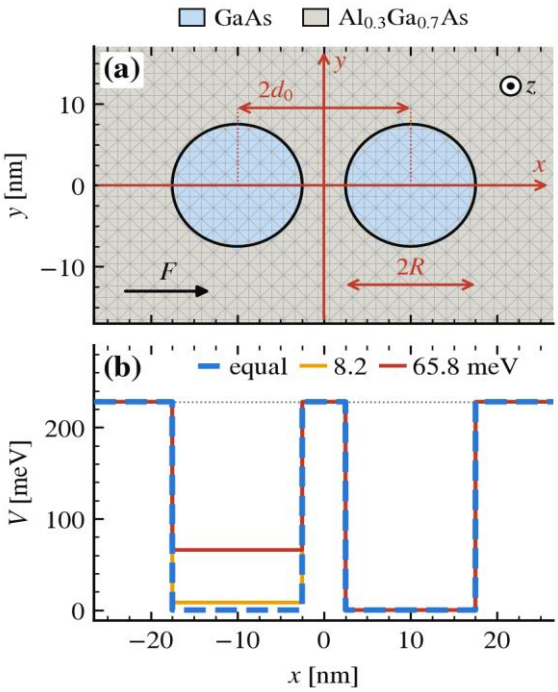



***Fig. 1.*** *(a) Cross section in the $x$–$y$ plane. (b) Confinement potential $V$ along the line $y = 0$. The dotted line indicates the barrier height $V_0$.*

With $\rho_{L,R} = \sqrt{(x \pm d_0)^2 + y^2}$, the confinement potential is

$$V(x,y) = \begin{cases} V_L, & \rho_L \le R, \\ 0, & \rho_R \le R, \\ V_0, & \text{otherwise.} \end{cases} \quad (2)$$

where $V_0$ is the conduction-band offset and $V_L$ is the confinement offset of the left wire. Energies are measured from the potential floor of the right wire. Lengths are measured in the effective Bohr radius $a^* = 4\pi\varepsilon_0\varepsilon_r\hbar^2/(m^*e^2)$ and energies in the effective Rydberg $\mathrm{Ry}^* = m^*e^4/[2(4\pi\varepsilon_0\varepsilon_r\hbar)^2]$. In these units, Eq. (1) becomes

$$H = -\nabla^2 + V(x,y) + fx - \frac{2}{|\mathbf{r}-\mathbf{r}_i|}, \quad (3)$$

where $f = \frac{ea^*F}{\mathrm{Ry}^*}$ is the field in reduced units.

We study three configurations: the equal pair, $V_L = 0$, and two detuned pairs with $V_L = 8.2$ and 65.8 meV (1.43 and 11.51 $\mathrm{Ry}^*$). Figure 1(a) shows the cross section with the finite-element mesh, coarsened for display; elements whose centroids lie inside the circles are assigned to GaAs and are shaded. Figure 1(b) shows the

confinement potential of the three configurations along $y = 0$.

In the absence of the donor, the subband states follow from

$$H_\perp \psi_n = E_n \psi_n, \tag{4}$$

$$H_\perp = -\nabla_\perp^2 + V(x,y) + fx, \tag{5}$$

where $\psi_n$ and $E_n$ are the subband states and energies, $\nabla_\perp^2$ is the Laplacian in the $x$–$y$ plane, and $\psi_0$ and $E_0$ are the lowest subband state and energy in the presence of the field. We define the transfer field $F^*$ as the field at which $E_0$ reaches its maximum; at this field the electron moves from one wire to the other.

For the donor, we use the product trial function

$$\Psi(\mathbf{r}) = N\varphi(x,y)e^{-z^2/\lambda^2}, \tag{6}$$

where $\lambda$ is the variational parameter, which sets the axial extent of the donor state along $z$, and $N = (2/\pi\lambda^2)^{1/4}$ for a normalized $\varphi$. We adopt the Gaussian-type trial function of Radu and Niculescu [14] for donors in coaxial QWWs, with one difference: $\varphi$ is obtained in the presence of the donor (Eq. (9)) rather than taken as the donor-free subband state. The binding energy is defined as the ground-state energy of the system without the impurity minus that with the impurity:

$$E_b = E_0 - E_i, \tag{7}$$

$$E_i = \min_\lambda \frac{\langle \Psi|H|\Psi\rangle}{\langle \Psi|\Psi\rangle}. \tag{8}$$

The $z$ integration is carried out analytically. For each $\lambda$, $\varphi$ is then the ground state of

$$[H_\perp + V_{\text{eff}}]\varphi = E_\perp(\lambda)\,\varphi, \tag{9}$$

$$V_{\text{eff}}(x,y;\lambda) = -\frac{2}{\lambda\sqrt{\pi/2}}\, e^{\rho^2/\lambda^2} K_0(\rho^2/\lambda^2), \tag{10}$$

where $E_\perp(\lambda)$ is the lowest eigenvalue of Eq. (9), $\rho^2 = (x - x_i)^2 + y^2$ and $K_0$ is the modified Bessel function of the second kind. The donor energy is $E_i = \min_\lambda[E_\perp(\lambda) + \lambda^{-2}]$, where $\lambda^{-2}$ is the axial kinetic energy.

All eigenvalue problems in the $x$–$y$ plane are solved with the finite-element method using linear triangular elements [20,21], with a mesh spacing of 0.025 $a^*$ for donor-free and 0.02 $a^*$ for donor calculations. The lowest eigenvalues are obtained by sparse shift–invert iteration [22]. Each donor energy $E_i$ and its reference $E_0$ are evaluated on the same mesh. On these meshes, the equal-pair $E_0$ is 39.43 and 39.49 meV, respectively, which indicates the discretization uncertainty.

We use $m^* = 0.0665\, m_0$, $\varepsilon_r = 12.58$ and the conduction-band offset $V_0 = 228$ meV of an $Al_{0.3}Ga_{0.7}As$ barrier, as in Ref. [14]. These give $a^* = 10.01$ nm and $\text{Ry}^* = 5.72$ meV, so that $V_0 = 39.88\ \text{Ry}^*$ and $f = 1$ corresponds to $F \simeq 5.71$ kV/cm. The wire radius is $R = 7.51$ nm ($0.75\ a^*$), the centres are at $d_0 = 10.01$ nm ($a^*$), and the edge-to-edge separation is $d = 2d_0 - 2R = 5.01$ nm.

## RESULTS AND DISCUSSION

Figure 2 shows the confinement potential of the three configurations, with the ground-state density at $F = 0$ drawn above the ground-state energy $E_0$ on a common scale. In the equal pair, the ground-state energy is $E_0 = 39.43$ meV, and the probability density is distributed symmetrically between the wires (Fig. 2(a)). Raising the potential floor of the left wire localizes the ground state in the right wire (Fig. 2(b),(c)); for $V_L = 65.8$ meV, the raised floor lies above $E_0$. Because the floor of the right wire is unchanged, $E_0$ increases only slightly, to 39.60 meV for both $V_L = 8.2$ and 65.8 meV. This increase of 0.17 meV reflects the loss of interwire hybridization.

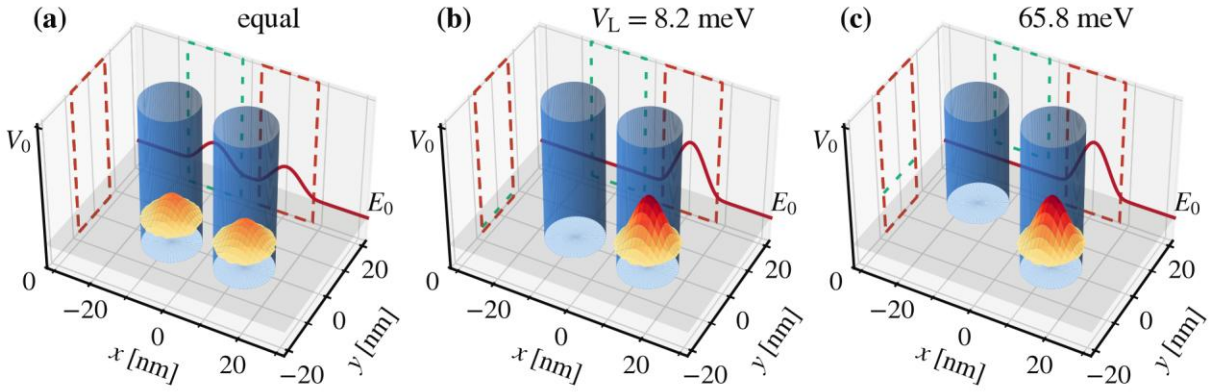



***Fig. 2.*** *Three-dimensional visualization of the confinement potential for (a) the equal pair and (b), (c) the detuned configurations with $V_L = 8.2$ and 65.8 meV. Dashed outlines on the $x$–$z$ and $y$–$z$ rear walls show orthogonal projections of the two wires (short dashes: left wire; long dashes: right wire). The grey plane marks $E_0$. The surface plotted above it represents $|\psi_0|^2$ at $F = 0$, using the same density scale in all three panels. The solid curve on the rear wall shows the density along $y = 0$.*

An electric field compensates the confinement offset. Figure 3 shows the $V_L = 65.8$ meV pair at three fields. At $F = 0$, the floor of the left wire lies 65.8 meV above that of the right wire, and the electron is localized in the right wire. The field tilts the potential and lowers the floor of the left wire relative to that of the right. At 31.35 kV/cm $\simeq F^*$, the floors at the two wire centres differ by only 3 meV, and the electron is shared almost equally between the wires, with a probability of 0.46 in the left wire.

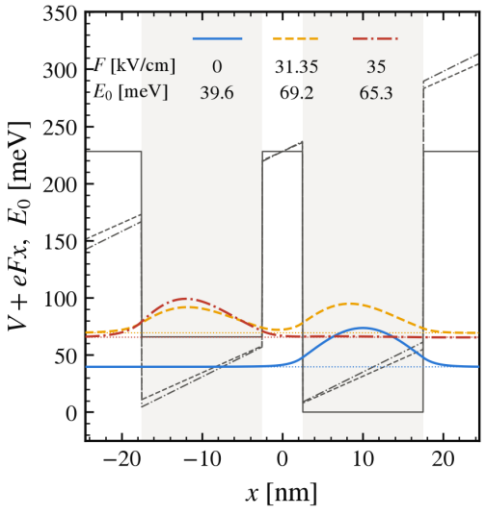



*Fig. 3. The $V_L = 65.8$ meV pair at $F = 0$ (blue), 31.35 kV/cm $\simeq F^*$ (yellow) and 35 kV/cm (red). Thin grey lines show the potential $V + eFx$ along $y = 0$, dotted lines the ground-state energies, and thick lines the scaled wavefunction sections $\psi_0(x, 0)$, with a common amplitude scale. The inset table lists $F$ and $E_0$. Shaded bands indicate the wires.*

At 35 kV/cm, the left floor lies 4.2 meV below the right one, and the electron is localized in the left wire. Since the field now lowers the occupied wire, $E_0$ decreases from 69.2 to 65.3 meV. The transfer takes place within a narrow field range: between 31.35 and 35 kV/cm, the probability in the left wire rises from 0.46 to 0.999. Within each wire, the field also shifts the density towards the lower side of the tilted potential.

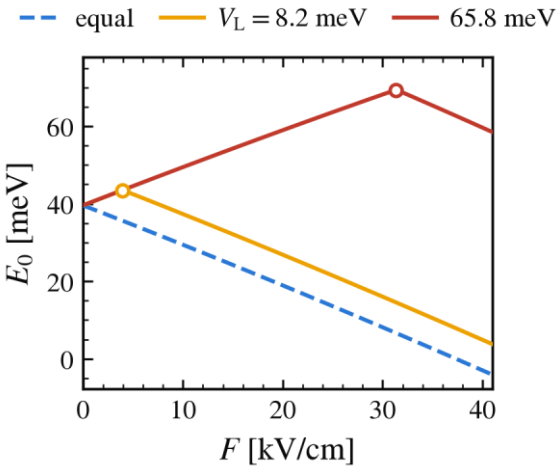



***Fig. 4.*** *Ground-state energy $E_0$ against the electric field for the three confinement configurations. Circles mark the energy maxima $F^*$ of the detuned pairs.*

Figure 4 shows the ground-state energy $E_0$ as a function of the field. For the equal pair, $E_0$ is largest at $F = 0$ (39.43 meV) and decreases with increasing field. For the detuned pairs, $E_0$ first increases at

approximately 1.00 meV per kV/cm; the two curves coincide in this range, since the electron is in the right wire. For $V_L = 8.2$ meV, $E_0$ increases up to 43.36 meV at 3.96 kV/cm and then decreases. For $V_L = 65.8$ meV, the maximum is 69.23 meV at 31.35 kV/cm. These maxima are the transfer fields $F^*$. At $F^*$, the field nearly compensates the offset: $2ed_0F^* = 7.9$ and 62.8 meV, compared with $V_L = 8.2$ and 65.8 meV. Beyond $F^*$, the electron is in the left wire, and $E_0$ decreases.

Figure 5 shows the donor energy and the binding energy. The donor is placed at $(x_i, 0,0)$, with $x_i$ varied from $-17.5$ to 17.5 nm (the outer wire edges) in steps of 0.5 nm along the line joining the wire centres. The dotted lines in Fig. 5(a) are the donor-free energies $E_0$, 39.49 meV for the equal pair and 39.7 meV for the detuned pairs. For the equal pair, $E_i$ has two minima of 20.9 meV at the wire centres, $x_i = \pm 10.0$ nm, and increases towards the barrier, where it reaches 31.7 meV, and towards the outer wire edges. The two minima are equal because the electron is distributed equally between the wires (Fig. 2(a)). For $V_L = 8.2$ meV, $E_i$ also has minima at both wire centres, but the minimum in the raised left wire (28.9 meV) lies above that in the right wire (20.9 meV). For $V_L = 65.8$ meV, there is a single minimum, at the centre of the right wire.

Since $E_0$ is nearly constant, $E_b = E_0 - E_i$ (Fig. 5(b)) mirrors $E_i$: the minima of $E_i$ appear as maxima of $E_b$. For the equal pair, $E_b$ has maxima of 18.6 meV at the wire centres, where the electron density is largest, a minimum of 7.8 meV in the barrier, and falls to 9.9 meV at the outer wire edges. In the right wire, the three profiles nearly coincide. For $V_L = 8.2$ meV, the maximum in the left wire is lowered to 10.8 meV. For $V_L = 65.8$ meV, $E_b$ has a single peak, in the right wire; in the left wire, it increases monotonically from 3.2 meV at the outer edge to 7.8 meV in the barrier. Related two-centre profiles have been reported for the laterally coupled rectangular wire pair of Tangarife and Duque [15], in which the asymmetry is introduced through unequal wire widths rather than unequal confinement depths.

To test the role of obtaining $\varphi$ in the presence of the donor, we repeated the calculation with $\varphi$ fixed to $\psi_0$, as in Ref. [14]. For the equal pair, $\psi_0$ is shared equally between the wires, so the electron cannot move towards the donor. The peak binding energy then falls from 18.6 to 10.9 meV, whereas the barrier value remains 7.8 meV, and the twin-peak profile flattens.

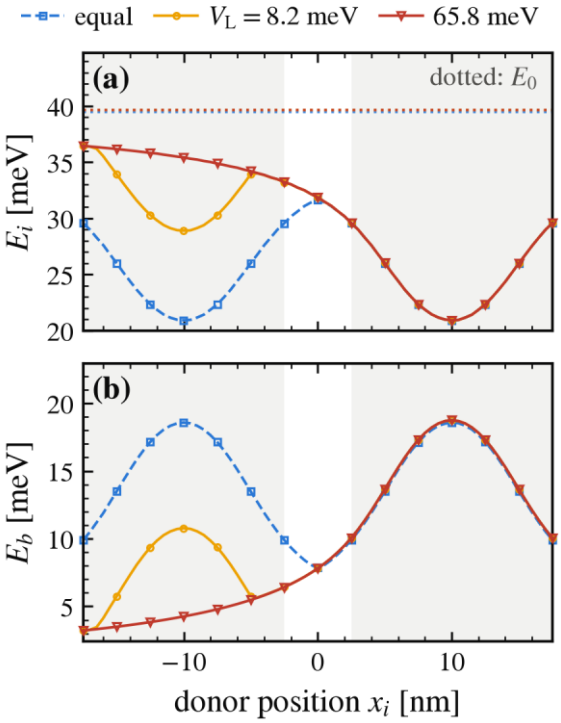



***Fig. 5.*** *Zero-field donor profiles along the line of centres for $V_L = 0$, 8.2 and 65.8 meV. The donor is at $(x_i, 0,0)$. (a) Variational donor energy $E_i$; dotted lines indicate the corresponding donor-free energies $E_0$, which nearly coincide on this scale. (b) Binding energy $E_b$. Shaded bands indicate the wires.*

The profiles in Fig. 5(b) reflect two kinds of variational solution. In one, the electron occupies the donor-containing wire (on-site binding). In the other, it remains in the deeper right wire and is bound to a donor in the left wire only through the barrier (across-barrier binding); for $V_L = 65.8$ meV, $E_b = 4.25$ meV at the left-wire centre. For $V_L = 8.2$ meV, the change from on-site to across-

barrier binding produces a local minimum of 5.7 meV near the inner edge of the left wire, at $x_i \approx -4.5$ nm. An applied field can restore strong binding to a donor in the raised wire by bringing the electron into that wire.

We next sweep the field with the donor held at the centre of the left wire, in the barrier and at the centre of the right wire (Fig. 6). The donor-present transfer field $F_d$ is the field at which the on-site and across-barrier solutions introduced above have equal energy, so that the electron moves to the other wire; at $F_d$, $E_b$ shows a kink.

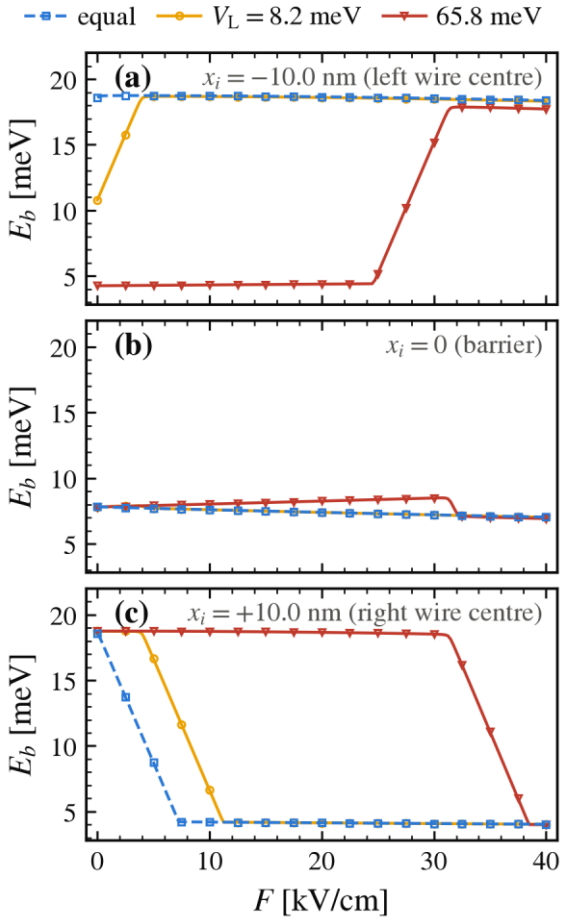



***Fig. 6.*** *Donor binding energy against the electric field for donors at (a) $x_i = -10.0$ nm, the centre of the left wire; (b) $x_i = 0$, the barrier; and (c) $x_i = 10.0$ nm, the centre of the right wire. The equal pair is shown by dashed curves with square markers; the $V_L = 8.2$ and 65.8 meV configurations use circles and triangles, respectively.*

For a donor at the centre of the left wire (Fig. 6(a)), the field moves the electron towards the donor. For the equal pair, the electron stays in the donor-containing wire, and $E_b$ remains between 18.4 and 18.8 meV. For $V_L = 8.2$ meV, the donor already holds the electron at zero field, with $E_b = 10.8$ meV; $E_b$ rises almost linearly to 18.6 meV at $F^* = 4.0$ kV/cm and then remains nearly constant. For $V_L = 65.8$ meV, $E_b$ stays near its across-barrier value of 4.3 meV up to $F_d = 24.6$ kV/cm, 6.7 kV/cm before $F^*$, then rises almost linearly to 17.9 meV near $F^*$ and remains nearly constant.

For a donor in the barrier (Fig. 6(b)), $E_b$ changes little, between 6.9 and 8.5 meV, since the donor is at the same distance from both wires. For the equal pair, it decreases monotonically from 7.85 meV at zero field to 7.03 meV at 40 kV/cm. For the detuned pairs, $E_b$ rises slightly up to the donor-free transfer field, reaching 7.90 and 8.49 meV for $V_L = 8.2$ and 65.8 meV, and then drops quickly; beyond $F^*$, the 8.2 meV curve nearly coincides with that of the equal pair. Here the calculation has a single solution at each field, so there is no $F_d$; the electron redistributes smoothly between the wires.

For a donor at the centre of the right wire (Fig. 6(c)), the electron initially occupies the donor-containing wire, and $E_b$ is 18.6–18.8 meV. $E_b$ starts to fall at the donor-free transfer field $F^*$, decreases almost linearly, and levels off at $F_d$ at 4.0–4.2 meV, the across-barrier value. $F_d = 7.3$, 11.2 and 38.5 kV/cm for the equal, 8.2 meV and 65.8 meV pairs, that is, 7.3, 7.3 and 7.2 kV/cm later than without the donor ($F^* = 0$, 4.0 and 31.3 kV/cm).

The shifts follow from an energy balance. Between $F^*$ and $F_d$, the electron occupies different wires with and without the donor, so $E_b$ changes almost linearly with the field, at a rate close to $2ed_0 = 2.00$ meV per kV/cm. The transfer therefore occurs when $2ed_0|F_d - F^*|$ equals the difference between the on-site binding at $F^*$ and the across-barrier binding at $F_d$. For the equal pair, $(18.6 - 4.2)$ meV divided by 2.00 meV per kV/cm gives 7.2 kV/cm, compared

with the computed 7.3 kV/cm; in the other three cases, the balance reproduces the computed shift within 0.2 kV/cm. These fields are variational estimates within the product trial function.

## CONCLUSION

Using the finite-element method within the effective-mass approximation, we have examined the ground state and donor binding of a laterally coupled cylindrical QWW pair in three configurations of the confinement offset, under an electric field.

(i) The electric field compensates the detuning and transfers the electron to the raised wire. For offsets of 8.2 and 65.8 meV, the ground-state energy reaches its maximum at $F^* = 3.96$ and 31.35 kV/cm, respectively, where $2ed_0F^*$ nearly equals the offset. This transfer field is obtained from the ground-state energy alone and does not require excited-state information.

(ii) The equal-pair donor profile has maxima of 18.6 meV at the wire centres and a barrier minimum of approximately 7.8 meV. Obtaining $\varphi$ in the presence of the donor is essential: with $\varphi = \psi_0$, the maxima fall to 10.9 meV. An offset of 8.2 meV lowers the maximum in the raised wire to 10.8 meV, and the profile remains two-centred. At 65.8 meV, this maximum is absent, and a donor on that side binds the electron only across the barrier, with $E_b = 4.25$ meV.

(iii) A fixed donor can shift the transfer field substantially. The magnitude of the shift is well approximated by the on-site minus across-barrier binding energy divided by $2ed_0$. Donors at the centre of the right wire delay transfer by 7.2–7.3 kV/cm in all three configurations; a donor at the centre of the left wire advances it by 6.7 kV/cm in the 65.8 meV configuration.

## REFERENCES


[1] W. G. van der Wiel, S. De Franceschi, J. M. Elzerman, T. Fujisawa, S. Tarucha, L. P. Kouwenhoven. Electron transport through double quantum dots. Rev. Mod. Phys. 2002;75:1-22. https://doi.org/10.1103/RevModPhys.75.1

[2] G. Burkard, T. D. Ladd, A. Pan, J. M. Nichol, J. R. Petta. Semiconductor spin qubits. Rev. Mod. Phys. 2023;95:025003. https://doi.org/10.1103/RevModPhys.95.025003

[3] T. Hayashi, T. Fujisawa, H. D. Cheong, Y. H. Jeong, Y. Hirayama. Coherent Manipulation of Electronic States in a Double Quantum Dot. Phys. Rev. Lett. 2003;91:226804. https://doi.org/10.1103/PhysRevLett.91.226804

[4] A. K. Hüttel, S. Ludwig, H. Lorenz, K. Eberl, J. P. Kotthaus. Direct control of the tunnel splitting in a one-electron double quantum dot. Phys. Rev. B 2005;72:081310. https://doi.org/10.1103/PhysRevB.72.081310

[5] L. DiCarlo, H. J. Lynch, A. C. Johnson, L. I. Childress, K. Crockett, C. M. Marcus, M. P. Hanson, A. C. Gossard. Differential Charge Sensing and Charge Delocalization in a Tunable Double Quantum Dot. Phys. Rev. Lett. 2004;92:226801. https://doi.org/10.1103/PhysRevLett.92.226801

[6] H. J. Krenner, M. Sabathil, E. C. Clark, A. Kress, D. Schuh, M. Bichler, G. Abstreiter, J. J. Finley. Direct Observation of Controlled Coupling in an Individual Quantum Dot Molecule. Phys. Rev. Lett. 2005;94:057402. https://doi.org/10.1103/PhysRevLett.94.057402

[7] G. J. Beirne, C. Hermannstädter, L. Wang, A. Rastelli, O. G. Schmidt, P. Michler. Quantum Light Emission of Two Lateral Tunnel-Coupled (In,Ga)As/GaAs Quantum Dots Controlled by a Tunable Static Electric Field. Phys. Rev. Lett. 2006;96:137401. https://doi.org/10.1103/PhysRevLett.96.137401

[8] J. Peng, C. Hermannstädter, M. Witzany, M. Heldmaier, L. Wang, S. Kiravittaya, A. Rastelli, O. G. Schmidt, P. Michler, G. Bester. Heterogeneous confinement in laterally coupled InGaAs/GaAs quantum dot molecules under lateral electric fields. Phys. Rev. B 2010;81:205315. https://doi.org/10.1103/PhysRevB.81.205315

[9] J. A. Vinasco, A. Radu, E. Kasapoglu, R. L. Restrepo, A. L. Morales, E. Feddi, M. E. Mora-Ramos, C. A. Duque. Effects of Geometry on the Electronic Properties of Semiconductor Elliptical Quantum Rings. Sci. Rep. 2018;8:13299. https://doi.org/10.1038/s41598-018-31512-4

[10] C. Heyn, C. A. Duque. Donor impurity related optical and electronic properties of

cylindrical GaAs-AlxGa1-xAs quantum dots under tilted electric and magnetic fields. Sci. Rep. 2020;10:9155. https://doi.org/10.1038/s41598-020-65862-9
[11] C. M. Duque, J. D. Correa, A. L. Morales, M. E. Mora-Ramos, C. A. Duque. Laterally coupled circular quantum dots under applied electric field. Physica E 2016;77:34-43. https://doi.org/10.1016/j.physe.2015.10.024
[12] G. W. Bryant. Hydrogenic impurity states in quantum-well wires. Phys. Rev. B 1984;29:6632-6639. https://doi.org/10.1103/PhysRevB.29.6632
[13] E. C. Niculescu, A. Radu. Binding energy of an off-center donor in cylindrical quantum-well wires under intense laser fields. U.P.B. Sci. Bull. Series A 2008;70(1):67-76.
[14] A. Radu, E. C. Niculescu. Intense THz laser effects on off-axis donor impurities in GaAs-AlGaAs coaxial quantum well wires. Phys. Lett. A 2010;374:1755-1761. https://doi.org/10.1016/j.physleta.2010.02.007
[15] E. Tangarife, C. A. Duque. Shallow-donor impurity in coupled GaAs/Ga1-xAlxAs quantum well wires: hydrostatic pressure and applied electric field effects. Phys. Status Solidi B 2010;247:1778-1785. https://doi.org/10.1002/pssb.200945519
[16] E. Tangarife, C. A. Duque. Combined effects of hydrostatic pressure and electric field on the donor binding energy and polarizability in laterally coupled double InAs/GaAs quantum-well wires. Appl. Surf. Sci. 2010;256:7234-7241. https://doi.org/10.1016/j.apsusc.2010.05.057
[17] P. Ulloa, M. Pacheco, Z. Barticevic, L. E. Oliveira. Effects of applied electric and magnetic fields on a donor impurity in laterally coupled quantum dots. J. Phys.: Condens. Matter 2011;23:325301. https://doi.org/10.1088/0953-8984/23/32/325301
[18] Ş. Aktaş, S. E. Okan, H. Akbaş. Electric field effect on the binding energy of a hydrogenic impurity in coaxial GaAs/AlxGa1-xAs quantum well-wires. Superlattices Microstruct. 2001;30:129-134. https://doi.org/10.1006/spmi.2001.1004
[19] Ş. Aktaş, F. K. Boz, S. Şentürk Dalgıç. Electric and magnetic field effects on the binding energy of a hydrogenic donor impurity in a coaxial quantum well wire. Physica E 2005;28:96-105. https://doi.org/10.1016/j.physe.2005.02.002
[20] M. Ogawa, T. Kunimasa, T. Ito, T. Miyoshi. Finite-element analysis of quantum wires with arbitrary cross sections. J. Appl. Phys. 1998;84:3242-3249. https://doi.org/10.1063/1.368478
[21] D. B. Topalović, V. V. Arsoski, S. Pavlović, N. A. Čukarić, M. Ž. Tadić, F. M. Peeters. On Improving Accuracy of Finite-Element Solutions of the Effective-Mass Schrödinger Equation for Interdiffused Quantum Wells and Quantum Wires. Commun. Theor. Phys. 2016;65:105-113. https://doi.org/10.1088/0253-6102/65/1/105
[22] R. B. Lehoucq, D. C. Sorensen, C. Yang. ARPACK Users' Guide: Solution of Large-Scale Eigenvalue Problems with Implicitly Restarted Arnoldi Methods. Philadelphia: SIAM, 1998. https://doi.org/10.1137/1.9780898719628.